Article

pubs.acs.org/Biomac

Effects of Crystal Orientation on Cellulose Nanocrystals–Cellulose Acetate Nanocomposite Fibers Prepared by Dry Spinning

Si Chen,[†] Greg Schueneman,[‡] R. Byron Pipes,[†,§,∥] Jeffrey Youngblood,*[,§] and Robert J. Moon[‡,§]

[†]School of Chemical Engineering, [§]School of Materials Engineering, and [∥]School of Aeronautics and Astronautics, Purdue University, West Lafayette, Indiana 47907, United States

[‡]The Forest Products Laboratory, U.S. Forest Service, Madison, Wisconsin 53726, United States

Supporting Information

ABSTRACT: This work presents the development of dry spun cellulose acetate (CA) fibers using cellulose nanocrystals (CNCs) as reinforcements. Increasing amounts of CNCs were dispersed into CA fibers in efforts to improve the tensile strength and elastic modulus of the fiber. A systematic characterization of dispersion of CNCs in the polymer fiber and their effect on the nanocomposites' mechanical properties is described. The birefringence, thermal properties, and degree of CNC orientation of the fibers are discussed. 2D X-ray diffraction was used to quantify the degree of CNC alignment within the fibers. It is shown that the CNC alignment directly correlates to the mechanical properties of the composite. Maximum improvements of 137% in tensile strength and 637% in elastic modulus were achieved. Empirical micromechanical models Halpin–Tsai equation and an orientation modified Cox model were used to predict the fiber performance and compared with experimental results.

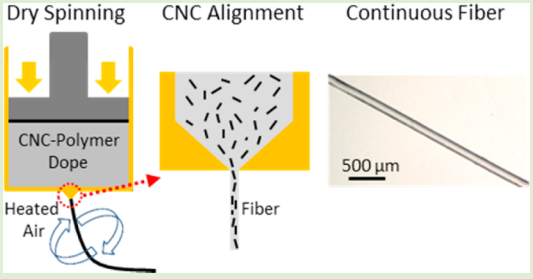

INTRODUCTION

Cellulose nanocrystals (CNCs) are rod-like nanoparticles (diameter ∼ 5–20 nm, length ∼ 50–500 nm) produced by controlled acid hydrolysis of cellulose-based materials such as plants and trees.[1−4] CNCs have been studied as a reinforcement phase in a wide variety of composite systems[2,5−7] due to attractive traits such as high aspect ratio, high mechanical properties,[8] low density, low coefficient of thermal expansion,[9] and surfaces accessible to chemical functionalization. CNCs also exhibit anisotropic mechanical properties, in which the elastic moduli in the long axis of the particle is much higher (110–220 GPa[1,10]) than in the transverse directions (2–50 GPa[10,11]). The ramification of this anisotropy is that, by controlling the CNC alignment during processing, one can obtain greater stiffening effects for a given amount of CNC addition.

Shear deformation is one method used to induce CNC alignment.[8,12,13] Under shear, due to their rod-like shape, CNCs naturally align along the shear direction, which decreases their flow resistance. As a result, the mechanical properties of the composite in the direction of the CNC alignment can be greatly increased. Fiber spinning is one processing technique that can generate such high shear rates. CNCs have been used in fiber spinning of various polymer systems via electrospinning[14−25] and wet or gel spinning.[26−32] The spinning process consists of a polymer dissolved in solvent extruded through a device containing small orifices known as the spinneret. The filaments then may be passed through air or liquids to solidify, known as dry or wet spinning, respectively. For electrospinning, high voltage is applied between the orifice and a "target" that effectively accelerates the jet of solution to the target. In most studies, the addition of CNCs has resulted in an increase in mechanical properties, as summarized in Figure 1. Electrospun CNC–polymer composite fibers report a typically low concentration of CNC loading (less than 20 wt %), and as compared to the neat polymer fiber, there is an increase in mechanical strength and elastic modulus in the fiber direction. However, mechanical properties were tested on fiber mats instead of single fibers and, as a result, are highly dependent on the mat configuration (number and alignment of the fibers).

To date wet spun CNC fibers have been produced via laboratory scale syringe pump systems, in which the resulting fibers (60–250 μm in diameter) have up to 50 vol % CNC loadings,[26] and CNC alignment in the fiber direction.[33] In most cases, the addition of CNCs increased mechanical properties of individual fibers (Figure 1). Liu et al.[29] wet spun CNC-artificial silk fibers, reporting a 3× increase in modulus and tensile strength at 5 wt % CNC loading. The same group wet spun CNC/regenerated cellulose fibers (0–9 wt % CNC loadings),[30] resulting in an increase in both the tensile strength (from 172 to 571 MPa) and the elastic modulus (from 2.06 to 4.15 GPa). Iwamoto et al.[33] wet-spun fibers made from 100% cellulose nanofibrils (CNF) and observed a direct relationship between shear rate, CNF alignment, and mechanical strength. Similar trends were reported by Hakansson et al.[34] for CNF fibers and

Received: August 7, 2014
Revised: September 15, 2014
Published: September 16, 2014

 © 2014 American Chemical Society

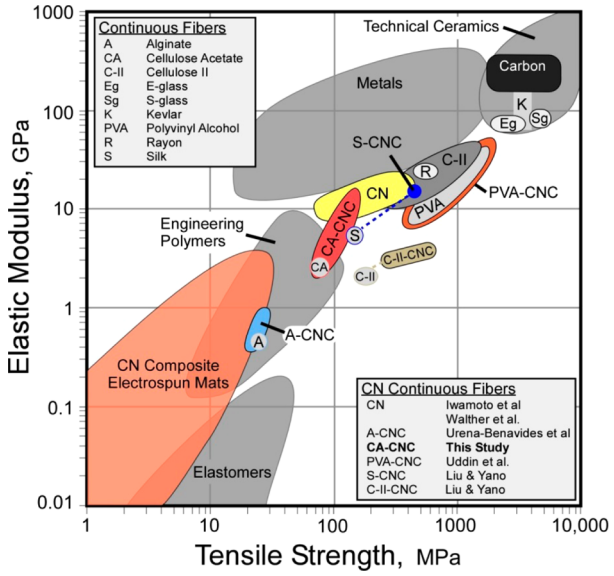

Figure 1. Overview of elastic modulus vs tensile strength of various cellulose nanomaterial (CN)−polymer filaments reported in literature and other common filament materials. Colored regions indicate studies containing CN or CNCs. The red region, CA-CNC, indicates results from this study.

by Urena-Benavides et al.[26−28] for CNC-alginate fibers containing up to 50 wt % CNC. Despite these improvements in mechanical properties by the addition of CNCs, these experimental values are lower than micromechanical model prediction for composite properties, suggesting improvements are possible.

Cellulose acetate (CA) is a semisynthetic polymer obtained from esterification of cellulose. CA fibers, typically produced by dry-spinning, are a commonly used product in clothing, filters, and diapers. There have been some recent attempts to improve the mechanical properties of CA including compounding it with clay,[35] modified and unmodified nanoclays,[36] and organoclays.[37] In these studies, tensile strength and modulus were increased 33−38% and transparency levels were decreased. As far as we know, there are no reports on dry or wet spun CA-CNC fiber systems. Herrera et al.[15] electrospun cellulose acetate fibers reinforced with wood CNC between 1 and 5 wt % concentrations. The maximum modulus of the electrospun fiber mat reported was 825 MPa at 1 wt % CNC, a 981% increase from the neat polymer fiber mat. No tensile strength data was reported. For CA-CNC films, Yang et al.[38] investigated the role of CNC concentration (2−7 wt % CNC) on the film mechanical properties. The maximum properties were observed at 4.5 wt % CNC with a 9% increase (44 MPa) in tensile strength and a 39% increase (1.5 GPa) in elastic modulus respective to the neat film properties.

In the present study, CA-CNC continuous fibers were produced via dry spinning. The role of CNC concentration and CNC alignment on the processing and resulting mechanical properties were investigated. Experimental results were compared to predictions from micromechanical models that accounted for CNC concentration, orientation state, and aspect ratio.

EXPERIMENTAL SECTION

Materials. Cellulose acetate (CA), with an acetyl content of 39.7 wt % should be on same line and an average molecular weight of 50000, was purchased from Sigma-Aldrich Chemistry. Reagent grade acetone (Sigma-Aldrich) and *N,N*-dimethylacetamide (DMAc) were used without further purification as the solvent.

Water-based suspensions of CNCs were produced and supplied by the USDA Forest Service-Forest Products Laboratory, Madison, WI.[4,39] The morphology of individual CNC particles was characterized via transmission electron microscopy (TEM; Philips CM-100, at 100 kV, spot 3, 200 μm condenser aperture, and 50 μm objective aperture) of CNC particles deposited on TEM grids (400 mesh Formvar/carbon filmed grid prepared with blow discharge) with 2% aqueous uranyl acetate stain. The average diameter (6 ± 2 nm) and length (83 ± 43 nm) of 93 individual CNC crystals were determined using ImageJ. A TEM image of CNCs can be found in the Supporting Information.

Methods. *Preparation of CA-CNC Solutions.* Water-based suspensions of CNCs were solvent exchanged into DMAc by vacuum-assisted rotary evaporation. Equal volumes of aqueous CNC dispersions and DMAc were mixed together in a round-bottom flask with agitation. Water and small amounts of DMAc were evaporated using the rotary evaporator (Yamato RE500) until the final volume was less than half of the initial volume. The final weight percentage of CNC in the dispersion was determined gravimetrically after drying the solution under vacuum at 80 °C for 24 h.

The dope solutions were prepared by dissolving the desired amount of CA in a mixture of acetone and DMAc. Varying amounts of CNC/DMAc dispersion were then added to obtain the desired CNC/CA concentration in the solutions. The solutions were agitated overnight and spun into fibers within 3 days of preparation.

Preparation of CA-CNC Fibers. The prepared solutions were dry-spun using a custom built plunger style fiber spinner based on a capillary viscometer[40] with spinneret insert having a 30° conical V-taper machined to a 4.38 mm for a 250 μm orifice (Bird Precision). This allows processing at shear rates similar to industrial processes (10^5−10^6/s) that is much higher than typical laboratory scale setups (10−10^2/s). The spinner was attached to a universal tensile testing machine (MTS Insight) to control displacement rate and measure pressure. The solutions and the stainless steel spinneret were heated to the operating temperature (65−95 °C) and held at temperature for 1 h for degassing purposes. The spinneret was mounted onto the MTS with counter current heated air at the spinner orifice (Figure 2). The dope solution was loaded into the spinneret, and the spinning process was started by pressing the plunger into the reservoir at maximum crosshead speed (1500 mm/min) until flow began. The continual spinning rate was regulated by the minimum amount of force needed

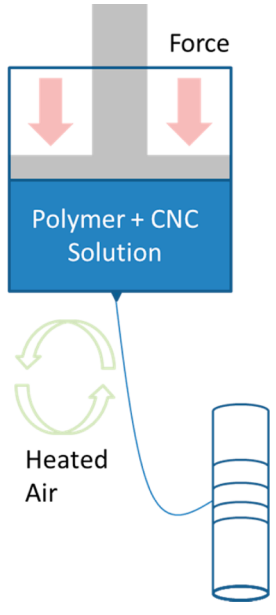

Figure 2. Schematic of the dry fiber spinning experimental setup.

dx.doi.org/10.1021/bm501161v | *Biomacromolecules* 2014, 15, 3827−3835

to maintain fiber flow. The fibers were then manually collected and further dried under vacuum at 3.4 kPa and 40 °C overnight. CA-CNC nanocomposite fibers were prepared with CNC concentrations of 0, 1, 2.5, 4, 8, 10, 14, 17, 20, 24, 29, 34, 39, 44, and 49 wt %. TGA experiments were carried out to ensure the final fiber contained no more than 5 wt % solvents. Exact experimental parameters are listed in the Supporting Information.

Rheology. Rheology experiments were performed on all suspensions using a TA Instruments AR-G2 rheometer. The steady state viscosity of the suspensions at room temperature was determined using parallel plate geometry at shear rates ranging from 0.1 to 100 s^{-1}.

Microscopy. Optical microscopy (OM; Olympus ZX-12) was used to observe the diameter and the surface morphology of the fibers. Optical images of each test specimen were taken. The diameters of the fibers were measured using the measure tool in ImageJ. Flow birefringence of CNCs within the fibers was observed in a Carl Zeiss (Axio Observer A1) inverted microscope with cross-polarizers. Scanning electron microscopy (SEM; FEI, XL40, at 5 kV) was used for close surface and cross section observation. All samples were coated in gold/palladium for 30 s at 1 kV, 18 mA, in a sputter coater (Hummer 6.2) prior to observation to minimize charging effects.

2D X-ray Diffraction. Two-dimensional wide-angle X-ray diffraction (2DWAXD; Bruker D8 GADDS, 546 nm Cu Kα radiation source at 40 mA, 20 kV for 600 s and a beam diameter of 500 μm in transmission mode) was used to study the degree of CNC alignment within the fibers. Multiple fibers (10−15) of the same CNC content were attached in a parallel bundle across a disk shaped fiber holder with a central opening. The holder was then placed perpendicular to the beam to allow the X-rays to pass through only the fibers. The WAXD patterns were recorded on a High Star 2D detector located 67 mm should be on same line from the sample. The patterns were corrected for air scattering and background by subtracting a no-fiber diffraction pattern from the raw data. Furthermore, a diffraction pattern containing only CA fibers was subtracted from all patterns of CA-CNC fibers in order to deconvolute the two components.

According to literature,[27] the distribution of intensity (I) with respect to ϕ along the arc that refers to the (200) reflections of the cellulose Iβ crystals[41] can be used to quantify the orientation of the CNC rods along the fiber axis. This peak is determined to be within 2θ = 21.0−22.3°. The integrated intensity with respect to ϕ was obtained by scanning along the arc from 0 to 180° around the (200) plane. Furthermore, Herman's order parameter (S) was calculated assuming axisymmetric orientation.[42] An order parameter of S = 0 indicates complete randomness of the CNCs arrangement within the fiber, while S = 1 indicates complete alignment of the CNCs along the fiber axis. The equations used in these calculations are listed in the Supporting Information.

Mechanical Testing. The tensile elastic modulus, ultimate strength, and strain at failure were measured using a dynamic mechanical analysis machine (TA Instruments, Q800). At least 10 fiber segments were randomly selected from specimens of each CNC concentration. "C" shaped tabs with adhesives were used to attach the samples to the DMA and avoid pinching at end points. Optical microscopy was used to determine the diameter of each and ensure there were no obvious defects. Fibers are assumed to be cylindrical in cross section as supported by optical imaging. Single fibers were tested with a gauge length of 30 mm, a constant applied force rate of 0.3 N/min at room temperature and relative humidity of 40 to 50% until fracture. Specimens that failed outside of the gauge length were considered improperly loaded, and were discarded in the data analysis.

Modeling. Several micromechanical models were used to estimate the elastic modulus of CA-CNC fibers as a function of CNC loading: Isostrain, isostress, Halpin−Tsai, and a modified Cox model. Isostrain and isostress are basic micromechanical models of idealized geometries. They assume the reinforcing filler of the composites are continuous and perfectly collimated in one direction, and there is perfect adhesion between the filler and the polymer matrix. The Halpin−Tsai model is an analytical form of Hill's generalized self-consistent model for composite materials. It takes into account short fibers and aspect ratios. The fillers are assumed to be collimated, and there is perfect adhesion between the filler and the polymer matrix. The modified Cox model takes porosity and orientation effects into account to predict the Young's modulus of the fiber composites. More details can be found in the Supporting Information.

RESULTS AND DISCUSSION

Spinning Solution Rheological Properties. The viscosities of the spinning solutions were measured to predict optimal conditions for fiber formation within the spinning system. It is well-known that CNCs exhibit shear thinning behavior in the dilute regime. At high shear rates, the CNCs align due to their rod-like shape and thereby greatly decrease the shear viscosity of the solution.[43] However, at higher concentrations, the suspensions transition into a gel-like material.[44] Considering this, the viscosity of the spinning solution should be a balance of the concentration of the polymer, viscosity of the polymer, the amount and orientation of CNCs, and the mixture of solvents in the solution.

The shear rate under typical industrial dry spinning processes can reach up to between 10^5 and 10^6 s^{-1}. It is difficult to achieve such shear rates in a rheometer, thus only general trends at relatively high shear was investigated. The Power Law model was applied to the rheology behaviors of the samples. The solutions presented a pseudoplastic behavior with a strong decline in apparent viscosity as shear rate increased. The addition of CNCs to the solutions did not alter the value of n. All solutions resulted in a flow behavior index value between 0.29 and 0.37. The change in the apparent viscosity was largely driven by the consistency coefficient, K, which is in essence the viscosity of the solution.

Experimental observations showed that when solutions with lower viscosities were extruded from the orifice, droplets were formed rather than a continuous/stable fiber. In contrast, stable fibers could be formed with high viscosity solutions, however, there is a potential for the formation of porosity defects within the fibers due to the inability for air pockets to quickly rise to the surface before solidification. With the dry spinning configuration used in this study, typically the critical viscosity of the dope solution for the formation of continuous fiber was ~10 Pa·s at 10 s^{-1} (Figure 3). The viscosity for pure 5.7 wt %

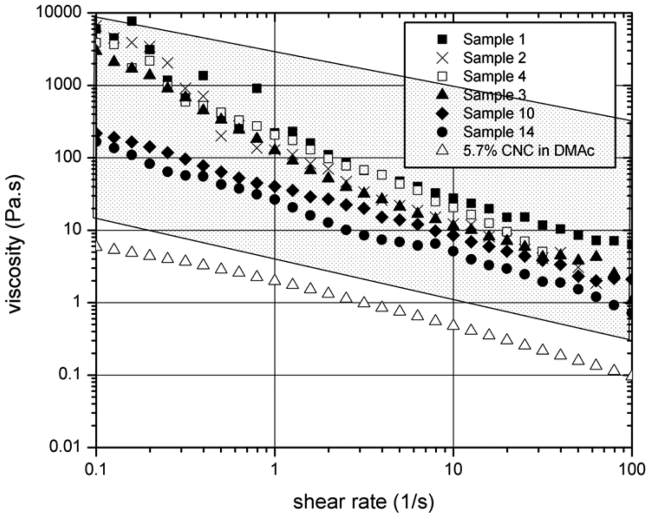

Figure 3. Viscosity vs shear rate data of various solutions. The shaded zone shows the approximate viscosity range at which the solutions formed fibers.

dx.doi.org/10.1021/bm501161v | Biomacromolecules 2014, 15, 3827−3835

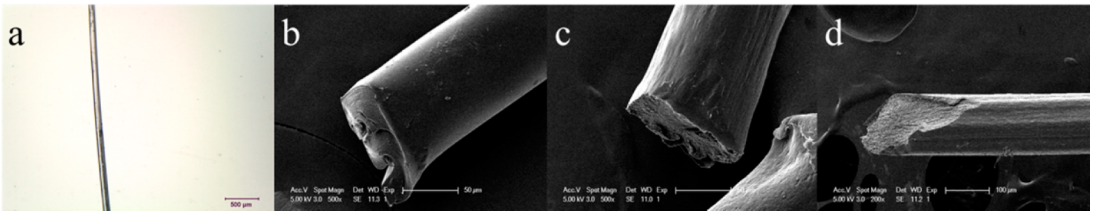

Figure 4. Optical microscopy image of (a) 17 wt % CA-CNC fiber, SEM images of (b) CA fiber, (c) 10 wt % CA-CNC fiber, and (d) 44 wt % CA-CNC fiber.

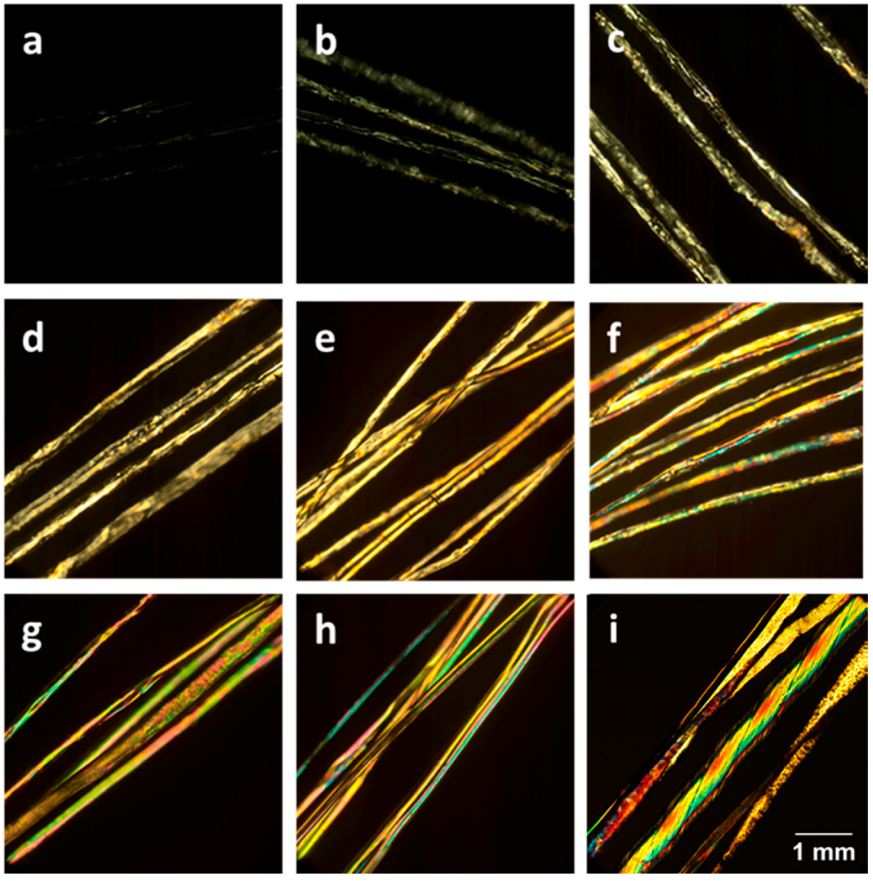

Figure 5. Image of CA-CNC fibers between cross polarizers: (a–i) contains CNC wt % of 0, 1, 2.5, 4, 10, 17, 24, 29, and 34%, respectively.

CNC in DMAc solution was too low to produce continuous fibers and thus 100 wt % CNC fibers could not be produced. However, continuous CA-CNC fibers were produced at 49 wt % CNC, which is the highest CNC concentration reported to date in CA-CNC composites.

CA-CNC Fiber Surface Morphologies. Figure 4 shows OM and SEM images of the CA-CNC fiber composites. The fibers were generally smooth on the surface and cylindrical in cross-section. Some defects observed were air voids, surface irregularities, and noncylindrical fiber cross sections. Porosity within the fibers was more common with higher viscosity dope solutions. Possible causes of the surface unevenness and deviations from cylindricality in the fiber cross-section may include clogging at the orifice or uneven drying conditions. More surface defects were observed at higher CNC concentrations. This may result from the addition of DMAc along with CNCs to the system. DMAc has a significantly higher boiling point than acetone (165 vs 57 °C), thus, greatly reducing the rate of solidification of the fibers, allowing more time for introduction of defects into the system.

As expected, the fracture surface of the neat CA fiber showed plastic deformation (Figure 4b). The addition of CNCs introduced brittleness into the fibers; this is evident in Figure 4d. Additionally, while smaller CNC agglomeration may still exist, at 1000× magnification, we do not see any large scale micron sized CNC agglomerates.

The CA fibers have an average diameter of 70 μm. The diameters of CA-CNC fibers were generally consistent, varying between 130 and 170 μm. The mechanism for the increased diameter is believed to be related, in part, from the additions of DMAc and CNCs in the solution. The addition of CNC increased the viscosity of the solution at low shear rates, resulting an overall larger fiber diameter due to increased resistance to gravitational stretching.

Birefringence Properties of CA-CNC Fibers. The dispersion and orientation of CNCs within the polymeric fibers was qualitatively studied with crossed polarizers. The two

dx.doi.org/10.1021/bm501161v | *Biomacromolecules* 2014, 15, 3827–3835

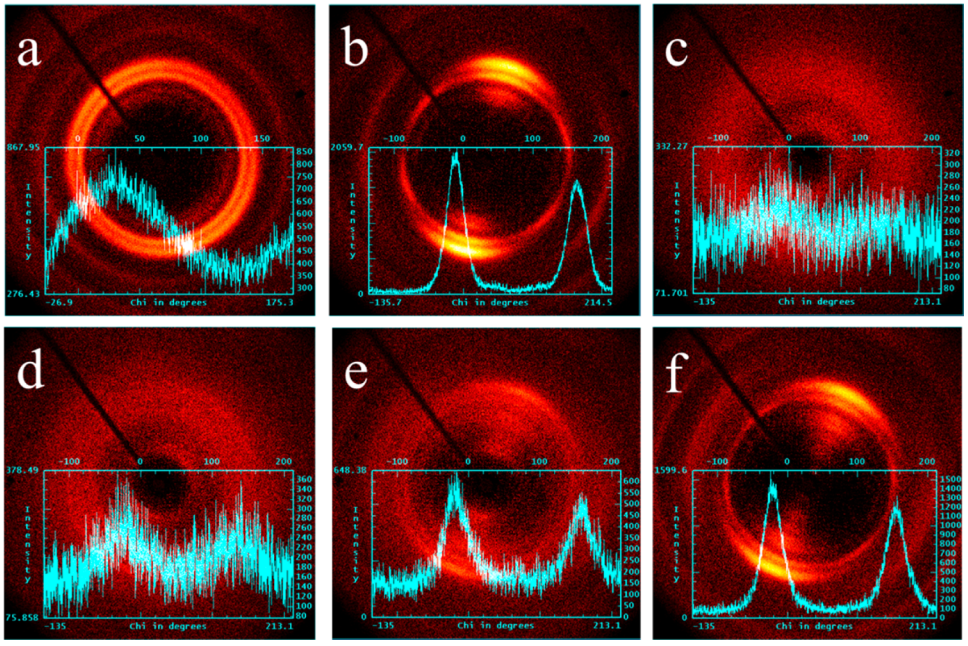

Figure 6. 2DXRD diffractograms of (a) a solution cast neat CNC film with randomly oriented CNCs, (b) shear cast neat CNC films with highly aligned CNC, and (c–f) are CA-CNC fibers with CNC contents of 0, 4, 17, and 34 wt %, respectively. The similarities between b and f indicate the 34 wt % CA-CNC is highly aligned.

polarizers placed at right angles would eliminate all light unless a birefringent material is placed between them at an angle, rotating the plane of linearized light. The highly crystalline CNCs are such a material, and the effect is constructive when the crystals become locally oriented. Crystalline CA is also birefringent, whereas amorphous CA is not. Figure 5 shows optical microscopy pictures of the fiber composites under the crossed polarizers. CA fibers show little to no birefringence, indicating the polymer remains mostly amorphous with a low degree of orientation after the spinning process (Figure 5a). An increase in the amount birefringence is observed with the addition of CNCs to the system. Isotropic CNCs, independent of CNC concentration, appear with some level of birefringence, regardless of the orientation of the sample with respect to the crossed polarizers, indicating randomness with some low levels of local orientation. When CNCs are globally oriented, this effect intensifies and the birefringence can be observed as bright colorful domains[44] whose intensity varies with respect to the orientation of the sample. This may be due to the liquid crystalline phase ordering with shear, as has been observed in CNC materials and films.[9] This effect is only achievable above a critical concentration of CNCs in the system, where there exist enough CNCs dispersed throughout the fibers to interact with each other. At low concentrations of CNC, the CNCs are mainly isotropic, with some local orientation appearing as clear with dark spots under the cross polarizers (Figure 5b,c). As the CNC concentration increases, birefringence also gradually increases until the entire fiber is bright with colorful domains (Figure 5d–i). This is indicative of well-dispersed and ordered CNCs within the CA matrix, where CNC agglomerates would be expected to appear as dark regions within the image. However, due to the magnification limits of the technique, only large micron scale agglomerations would be observable.

CNC Orientation within CA-CNC Fibers. The extent of CNC alignment along the fiber axis was quantified using 2D XRD and Herman's order parameter (S).[27,45] Figure 6 shows X-ray diffractograms and the integrated intensity of two cast pure CNC films; shear and self-organized, along with diffractograms of several fibers, increasing in CNC content. The self-organized CNC film (Figure 6a) showed uniform intensity around the Debye–Scherrer ring patterns, indicating a random orientation of CNCs in the horizontal plane of the film. The ordered CNC film (Figure 6b) showed two sharp intensity peaks along the arc, indicating the CNCs are aligned along the horizontal direction of the film-plane. The diffractogram of pure CA fibers (Figure 6c) showed minimum or low levels of orientation of the polymer chains. This particular diffraction pattern was subtracted from all CA-CNC diffraction patterns as a background in order to deconvolute the two components. In addition, % crystallinity of CA was determined to be low, regardless of CNC wt % using differential scanning calorimetry (see Supporting Information). For the CA-CNC fibers (Figure 6c–f), a clear trend of increasing sharp peaks along the (200) ring with increasing CNC content is observed, which is indicative of increasing CNC orientation along the fiber axis. Note if there were no changes in CNC alignment, then with increasing CNCs additions there would be an even/uniform increase in intensity along the entire (200) ring (i.e., for all ϕ).

The CNC alignment along the fiber axis increases with CNC concentration (Figure 7), in agreement with the birefringence observed in the OM images. There is an apparent plateau of the order parameter after 30 wt % CNCs, above which adding more CNCs did not further improve alignment along the fiber axis. Furthermore, the maximum achieved level of CNC alignment within the fibers was similar to that of the shear cast neat CNC films ($S \sim 0.7$),[8,9] despite the different methods and shear rates. This suggests there is a maximum level of orientation that can be achieved at a high concentration of CNC through shear forces. When this concentration is reached, the interactions between CNCs prevent further alignment. One possible mechanism proposed for nanoparticle reinforced composites suggests the nanoparticles aggregate together at high

dx.doi.org/10.1021/bm501161v | Biomacromolecules 2014, 15, 3827–3835

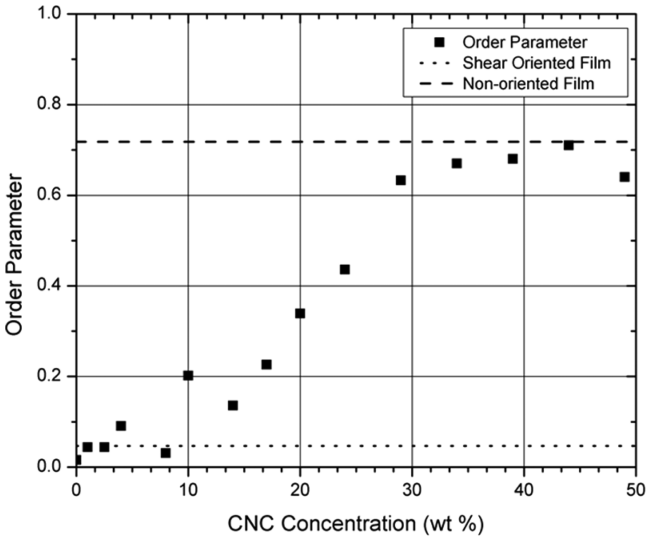

Figure 7. Herman's order parameter as a function of CNC content in fiber, showing that there is a corresponding increase in the order parameter for increasing CNC concentration up to a plateau of S = ~0.7 at a concentration of ~30 wt % CNC. The straight line indicates the order parameter of the shear oriented film, and the dashed line shows the order parameter of the randomly oriented film.

concentrations, forming a bundle. As a result of this behavior, further orientation of the CNCs is limited.[46]

CA-CNC Fiber Mechanical Properties. The mechanical properties of the nanocomposite fiber are shown in Figure 8.

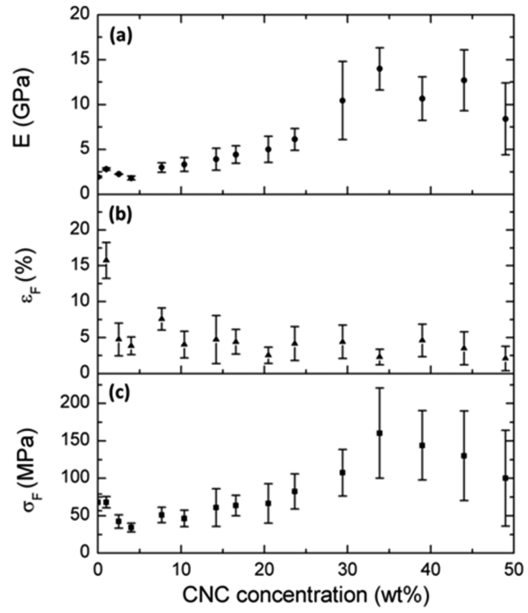

Figure 8. Mechanical properties of as-spun CA-CNC fibers, without post processing: (a) Young's modulus, (b) elongation at break, and (c) tensile strength as a function of CNC wt %.

The neat CA fiber has an elastic modulus of 1.9 GPa, a tensile strength of 67.7 MPa, and reached 34.5% elongation before failure. Industrial grade CA fiber properties range in 2.7−2.9 GPa for elastic modulus, 139−163 MPa for tensile strength and 25−45% for elongation.[47] It is important to stress that the fibers produced in the current study are not optimized by any post processing (washing, solvent extraction, drawing, and surface finishing), which could further improve properties.

In general, the elastic modulus and tensile strength increased up to a critical CNC concentration, after which point the properties plateau and slightly decreases with further addition of CNC. In both cases, the maximum value was reached at 34 wt % CNC (elastic modulus: 1.9 to 14.0 GPa, and strength: 67.7 to 160.3 MPa). The elongation at failure of the fibers decreased by the addition of CNCs. As observed from the SEM images of the fracture surfaces, the fibers become increasingly brittle with higher CNC concentration with failure at 45 ° to the fiber axis, indicating shear failure at the highest concentrations. The elongation at failure decreased quickly from at 35% for pure CA fibers to 5% with a small addition of CNC (2.5 wt %), and plateaus to 1−2% with CNC additions up to 49 wt %.

The role of CNC alignment in affecting mechanical properties is strongly correlated. The overall curve shape of the modulus and tensile strength plots corresponds directly to the orientation parameter curve in Figure 7. Thus, increasing CNC alignment in the fiber direction is an important factor for improvement of mechanical properties. As discussed before, CNCs are highly anisotropic. The axial Young's modulus of CNCs is 110−220 GPa, while the transverse is 2−50 GPa.[1] As the CNCs become more oriented along the fiber axis with increasing CNC concentration, a higher mechanical reinforcement from the CNCs is observed. This effect explains the exponential shape of both the modulus and the tensile strength curve from 0 to 30 wt %. Once the maximum level of orientation is achieved, the curve immediately plateaus. Any further addition of CNCs does not increase mechanical properties. Similarly, Urena-Benavides et al.[26−28] reported a plateau in mechanical performance above 10 wt % CNC-in alginate fibers produced via wet spinning from a laboratory scale syringe pump.

The plateau and increase scatter in the measurements at higher CNC loads (>34 wt %) suggest defect-mediated failure, in which the fiber prematurely fails either from the geometrical thinnest part or the structural weak point of the fiber. The primary types of defects associated with the fibers produced in this study are considered to result from CNC agglomeration, porosity within the fiber, and uneven fiber diameter and cross-sectional shape. It is possible that the amount and type of defects within the fibers increased as the CNC concentration increased above 34 wt %, as evident by SEM images. CNC agglomeration decreases the overall CNC-polymer interfacial area, which decreases the potential reinforcing effect of the CNCs, and causes the plateau at higher CNC concentrations. Porosity or air voids within the fiber not only decreases the effective cross-section, which decreases the measured modulus, but also creates stress concentrations within the fibers, leading to premature failure. Likewise, uneven cross-section and diameters also contribute to stress concentrations.

The increase mechanical property observed in the current study is similar to what was reported in previous CA-CNC composites studies.[15,38] Furthermore, to our knowledge, the critical concentration at which the maximum mechanical properties were achieved is higher than all studies reported on polymer−CNC fiber composites.[14−31,48−52] This demonstrates that by applying higher shear rates, the resulting increased CNC alignment within the fiber provided a mechanism to better utilize the CNC's reinforcing potential for properties along the fiber direction. A comparison of this

study to other CNC fiber reports and common filament materials is shown in Figure 1.

Micromechanical Modeling of CA-CNC Nanocomposite Fibers. Young's modulus predictions from the isostrain and isostress model, the modified orientation Cox model and the Halpin−Tsai equations for short fiber composites are shown in Figure 9. The isostrain and isostress models assume

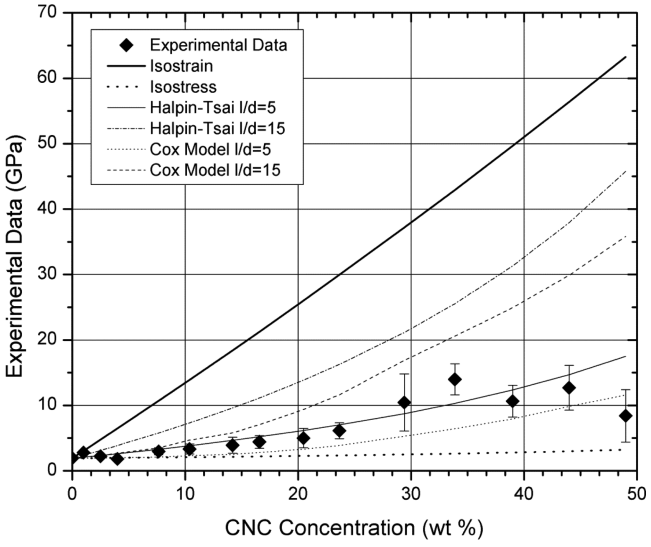

Figure 9. Predictions of the Young's modulus using isostrain, isostress, Halpin−Tsai equation, and the modified orientation Cox model with aspect ratios of 5 and 15 plotted along with experimental data.

all CNCs are continuous fibers that are either collimated along the fiber axis (isostrain) or perpendicular to it (Isostress). As expected, the isostrain case greatly overestimates the performance of the composite, and the isostress case underestimates it. Thus, these models provide the widest upper and lower bounds for the CA-CNC composite performance. The Halpin−Tsai equations provide refinement based on particle morphology by considering that CNCs are discrete short fibers and the role of CNC aspect ratio. The Cox model provides even further refinement by considering both CNC aspect ratio and alignment.

Using empirical fittings, an aspect ratio (L/D) of 5 using Halpin−Tsai equations gives the closest prediction to experimental values. An average value of 15 for aspect ratio was calculated from TEM data collected from CNC samples. As shown in Figure 9, using this aspect ratio over predicts the composites' performance. However, TEM data presents a very small sample size; thus, the experimentally obtained value may not necessarily be 100% representative. Nevertheless, one would expect the true aspect ratio to be higher than 5 since these equations do not take orientation and anisotropy of the fillers into consideration, assuming a perfect unidirectional filler orientation, where all CNC particle contributions are at axial Young's modulus values. Furthermore, the model assumes perfect adhesion between the CNC and matrix, which may not be realistic for the CA-CNC interface. It is also plausible that the wood CNCs exhibit an axial modulus lower than the 143 GPa assumed.[53] Any deviation from these assumptions would contribute to the model overpredicting the composite mechanical performance.

The CNC reinforcement effects are considered to increase as the particles become more aligned along the fiber axis. The modified orientation Cox model utilizes this additional information to give a more accurate microstructural representative of the CA-CNC composite and predict elastic properties based off of this structure. The results from the model are presented in Figure 9 for both aspect ratios of 15 and 5 serving as upper and lower bounds. The model predictions and experimental data are in good agreement until high concentrations of CNC (40−50 wt %), where composite performance is near or lower than the lower bound. This may be an indication of the increased interactions or agglomeration between the CNCs at a higher concentration.

Even though the models discussed here are simple approaches to predict mechanical reinforcement by CNCs, they demonstrate the importance of CNC dispersion and alignment. Increasing CNC past the optimum concentration could negatively impact CNC dispersion, limiting elastic modulus improvement as CNC concentration increases.

CONCLUSIONS

Cellulose acetate−cellulose nanocrystal (CA-CNC) fiber nanocomposites were produced using a dry spinning process. Continuous CA-CNC fibers of average diameter 150 μm and varying CNC concentrations between 0 and 49 wt % were produced. Tensile breaking strength and modulus were found to be greatly improved by CNC additions up to 34 wt %, after which the properties plateaued or decreased, possibly due to defect formation from a loss in CNC dispersion or residual pores. The fiber spinning process led to a shear induced alignment of the CNCs along the fiber axis. The degree of CNC alignment was shown to be one mechanism for altering the CA-CNC fiber mechanical properties in the fiber axial direction. Micromechanical models suggest that the increase in elastic modulus of the CA-CNC continuous fiber resulted from CNC concentration, orientation state and aspect ratio. We demonstrated the ability to produce CNC polymer nanocomposites with large improvements in mechanical properties. Maximum reinforcement of CNC additions occurred at 34 wt % CNC, in which the resulting improvements in tensile strength and elastic modulus were 137 and 637%, respectively. Furthermore, given the existing dry spinning commercial market, we believe the method described shows promising potential to be scaled up to a commercially viable fiber.

ASSOCIATED CONTENT

Supporting Information

Processing parameters for CA-CNC composite fibers, TEM image of CNCs, rheological power law model data, diameter, mechanical properties, and order parameters of CA-CNC composite fibers, Herman's order parameter calculations, micromechanical modeling equations, DSC thermograms, and stress−strain curves. This material is available free of charge via the Internet at http://pubs.acs.org.

AUTHOR INFORMATION

Notes

The authors declare no competing financial interest.

ACKNOWLEDGMENTS

This work has been supported by The U.S. Department of Defense, Air Force Office of Scientific Research (Grant No. FA9550-11-1-0162) and USDA Forest Service (Grant No. 11-JV-11111129-118). The authors thank Steve Lacher and Dave

Eustice at the USDA Forest Service, Forest Products Laboratory, for the design and processing of the spinner unit, respectively, and the material science department at Purdue University for support and the usage of characterization equipment.

REFERENCES

(1) Moon, R. J.; Martini, A.; Nairn, J.; Simonsen, J.; Youngblood, J. Cellulose nanomaterials review: structure, properties and nanocomposites. *Chem. Soc. Rev.* **2011**, *40*, 3941−3994.
(2) Samir, M. A. S. A.; Alloin, F.; Dufresne, A. Review of recent research into cellulosic whiskers, their properties and their application in nanocomposite field. *Biomacromolecules* **2005**, *6*, 612−626.
(3) Siro, I.; Plackett, D. Microfibrillated cellulose and new nanocomposite materials: a review. *Cellulose* **2010**, *17*, 459−494.
(4) Beck-Candanedo, S.; Roman, M.; Gray, D. G. Effect of reaction conditions on the properties and behavior of wood cellulose nanocrystal suspensions. *Biomacromolecules* **2005**, *6*, 1048−1054.
(5) Eichhorn, S. J.; Dufresne, A.; Aranguren, M.; Marcovich, N. E.; Capadona, J. R.; Rowan, S. J.; Weder, C.; Thielemans, W.; Roman, M.; Renneckar, S.; Gindl, W.; Veigel, S.; Keckes, J.; Yano, H.; Abe, K.; Nogi, M.; Nakagaito, A. N.; Mangalam, A.; Simonsen, J.; Benight, A. S.; Bismarck, A.; Berglund, L. A.; Peijs, T. Review: current international research into cellulose nanofibres and nanocomposites. *J. Mater. Sci.* **2010**, *45*, 1−33.
(6) Siqueira, G.; Bras, J.; Dufresne, A. Cellulose whiskers versus microfibrils: influence of the nature of the nanoparticle and its surface functionalization on the thermal and mechanical properties of nanocomposites. *Biomacromolecules* **2009**, *10*, 425−432.
(7) Lin, N.; Huang, J.; Dufresne, A. Preparation, properties and applications of polysaccharide nanocrystals in advanced functional nanomaterials: a review. *Nanoscale* **2012**, *4*, 3274−3294.
(8) Reising, A. B.; Moon, R. J.; Youngblood, J. P. Effect of particle alignment on mechanical properties of neat cellulose nanocrystal films. *J. Sci. Technol. For. Prod. Processes* **2013**, *2*, 32−41.
(9) Diaz, J. A.; Wu, X. W.; Martini, A.; Youngblood, J. P.; Moon, R. J. Thermal expansion of self-organized and shear-oriented cellulose nanocrystal films. *Biomacromolecules* **2013**, *14*, 2900−2908.
(10) Dri, F.; Hector, L., Jr.; Moon, R.; Zavattieri, P. Anisotropy of the elastic properties of crystalline cellulose Iβ from first principles density functional theory with van der Waals interactions. *Cellulose* **2013**, *20*, 2703−2718.
(11) Wagner, R.; Raman, A.; Moon, R. Transverse elasticity of cellulose nanocrystals via atomic force microscopy. *Cellulose* **2010**, *7*, 27.
(12) Orts, W. J.; Godbout, L.; Marchessault, R. H.; Revol, J. F. Enhanced ordering of liquid crystalline suspensions of cellulose microfibrils: A small angle neutron scattering study. *Macromolecules* **1998**, *31*, 5717−5725.
(13) Aguié-Béghin, V.; Molinari, M.; Hambardzumyan, A.; Foulon, L.; Habibi, Y.; Heim, T.; Blossey, R.; Douillard, R. Preparation of ordered films of cellulose nanocrystals. *Model Cell. Surf.* **2009**, *1019*, 115−136.
(14) Dong, H.; Strawhecker, K. E.; Snyder, J. F.; Orlicki, J. A.; Reiner, R. S.; Rudie, A. W. Cellulose nanocrystals as a reinforcing material for electrospun poly(methyl methacrylate) fibers: formation, properties and nanomechanical characterization. *Carbohydr. Polym.* **2012**, *87*, 2488−2495.
(15) Herrera, N. V.; Mathew, A. P.; Wang, L. Y.; Oksman, K. Randomly oriented and aligned cellulose fibres reinforced with cellulose nanowhiskers, prepared by electrospinning. *Plast., Rubber Compos.* **2011**, *40*, 57−64.
(16) Liu, D. Y.; Yuan, X. W.; Bhattacharyya, D. The effects of cellulose nanowhiskers on electrospun poly (lactic acid) nanofibres. *J. Mater. Sci.* **2012**, *47*, 3159−3165.
(17) Lu, P.; Hsieh, Y. L. Cellulose nanocrystal-filled poly(acrylic acid) nanocomposite fibrous membranes. *Nanotechnology* **2009**, *20*, 415604.
(18) Park, W. I.; Kang, M.; Kim, H. S.; Jin, H. J. Electrospinning of poly(ethylene oxide) with bacterial cellulose whiskers. *Macromol. Symp.* **2007**, *249*, 289−294.
(19) Peresin, M. S.; Habibi, Y.; Zoppe, J. O.; Pawlak, J. J.; Rojas, O. J. Nanofiber composites of polyvinyl alcohol and cellulose nanocrystals: manufacture and characterization. *Biomacromolecules* **2010**, *11*, 674−681.
(20) Rojas, O. J.; Montero, G. A.; Habibi, Y. Electrospun nanocomposites from polystyrene loaded with cellulose nanowhiskers. *J. Appl. Polym. Sci.* **2009**, *113*, 927−935.
(21) Xiang, C. H.; Joo, Y. L.; Frey, M. W. Nanocomposite fibers electrospun from poly(lactic acid)/cellulose nanocrystals. *J. Biobased Mater. Bioenergy* **2009**, *3*, 147−155.
(22) Zoppe, J. O.; Peresin, M. S.; Habibi, Y.; Venditti, R. A.; Rojas, O. J. Reinforcing poly(ϵ-caprolactone) nanofibers with cellulose nanocrystals. *ACS Appl. Mater. Int.* **2009**, *1*, 1996−2004.
(23) Lee, J.; Deng, Y. L. Increased mechanical properties of aligned and isotropic electrospun PVA nanofiber webs by cellulose nanowhisker reinforcement. *Macromol. Res.* **2012**, *20*, 76−83.
(24) Ago, M.; Jakes, J. E.; Johansson, L.-S.; Park, S.; Rojas, O. J. Interfacial properties of lignin-based electrospun nanofibers and films reinforced with cellulose nanocrystals. *ACS Appl. Mater. Int.* **2012**, *4*, 6849−6856.
(25) Vallejos, M. E.; Peresin, M. S.; Rojas, O. J. All-cellulose composite fibers obtained by electrospinning dispersions of cellulose acetate and cellulose nanocrystals. *J. Polym. Environ.* **2012**, *20*, 1075−1083.
(26) Urena-Benavides, E. E.; Brown, P. J.; Kitchens, C. L. Effect of jet stretch and particle load on cellulose nanocrystal-alginate nanocomposite fibers. *Langmuir* **2010**, *26*, 14263−14270.
(27) Urena-Benavides, E. E.; Kitchens, C. L. Wide-angle X-ray diffraction of cellulose nanocrystal-alginate nanocomposite fibers. *Macromolecules* **2011**, *44*, 3478−3484.
(28) Urena-Benavides, E. E.; Kitchens, C. L. Cellulose nanocrystal reinforced alginate fibers-biomimicry meets polymer processing. *Mol. Cryst. Liq. Cryst.* **2012**, *556*, 275−287.
(29) Liu, L.; Yao, J. M. Wet-spinning of reinforced artificial silk hybrid fibres by cellulose whiskers. *Adv. Mater. Res. (Durnten-Zurich, Switz.)* **2011**, *175*−*176*, 272−275.
(30) Liu, L.; Yao, J. M. Properties of biocomposite fibers from cellulose nanowhiskers and cellulose matrix. *J. Fiber Bioeng. Inform.* **2012**, *5*, 207−215.
(31) Uddin, A.; Araki, J.; Gotoh, Y. Toward strong green nanocomposites: polyvinyl alcohol reinforced with extremely oriented cellulose whiskers. *Biomacromolecules* **2011**, *12*, 617−624.
(32) Endo, R.; Saito, T.; Isogai, A. TEMPO-oxidized cellulose nanofibril/poly(vinyl alcohol) composite drawn fibers. *Polymer* **2013**, *54*, 935−941.
(33) Iwamoto, S.; Isogai, A.; Iwata, T. Structure and mechanical properties of wet-spun fibers made from natural cellulose nanofibers. *Biomacromolecules* **2011**, *12*, 831−836.
(34) Håkansson, K. M. O.; Fall, A. B.; Lundell, F.; Yu, S.; Krywka, C.; Roth, S. V.; Santoro, G.; Kvick, M.; Prahl Wittberg, L.; Wågberg, L.; Söderberg, L. D., Hydrodynamic alignment and assembly of nanofibrils resulting in strong cellulose filaments. *Nat. Commun.* **2014**, *5*.
(35) Wibowo, A. C.; Misra, M.; Park, H.-M.; Drzal, L. T.; Schalek, R.; Mohanty, A. K. Biodegradable nanocomposites from cellulose acetate: mechanical, morphological, and thermal properties. *Composites, Part A* **2006**, *37*, 1428−1433.
(36) Hassan-Nejad, M.; Ganster, J.; Bohn, A.; Pinnow, M.; Volkert, B. Bio-based nanocomposites of cellulose acetate and nano-clay with superior mechanical properties. *Macromol. Symp.* **2009**, *280*, 123−129.
(37) Rodríguez, F. J.; Coloma, A.; Galotto, M. J.; Guarda, A.; Bruna, J. E. Effect of organoclay content and molecular weight on cellulose acetate nanocomposites properties. *Polym. Degrad. Stab.* **2012**, *97*, 1996−2001.
(38) Yang, Z.-Y.; Wang, W.-J.; Shao, Z.-Q.; Zhu, H.-D.; Li, Y.-H.; Wang, F.-J. The transparency and mechanical properties of cellulose

acetate nanocomposites using cellulose nanowhiskers as fillers. *Cellulose* **2013**, *20*, 159−168.
(39) Reiner, R.; Rudie, A. *Process Scale-up of Cellulose Nanocrystal Production to 25 kg per Batch at the Forest Products Laboratory*; TAPPI Press: Peachtree Corners, GA, 2013.
(40) Salyer, I. O.; Heyd, J. W.; Brodbeck, R. M.; Hartzel, L. W.; Brown, L. E. Use of a capillary extrusion rheometer to measure curing of thermosetting plastics and rubbers. *J. Polym. Sci., Part A: Gen. Pap.* **1965**, *3*, 1911−1939.
(41) Nishiyama, Y.; Langan, P.; Chanzy, H. Crystal structure and hydrogen-bonding system in cellulose 1 beta from synchrotron X-ray and neutron fiber diffraction. *J. Am. Chem. Soc.* **2002**, *124*, 9074−9082.
(42) Advani, S. *Process Modeling in Composites Manufacturing*, 2nd ed. (Manufacturing Engineering and Materials Processing); CRC Press: New York, 2010; pp 132−134.
(43) Liu, D.; Chen, X.; Yue, Y.; Chen, M.; Wu, Q. Structure and rheology of nanocrystalline cellulose. *Carbohydr. Polym.* **2011**, *84*, 316−322.
(44) Revol, J. F.; Godbout, L.; Dong, X. M.; Gray, D. G.; Chanzy, H.; Maret, G. Chiral nematic suspensions of cellulose crystallites − phase-separation and magnetic-field orienation. *Liq. Cryst.* **1994**, *16*, 127−134.
(45) Park, S.; Baker, J. O.; Himmel, M. E.; Parilla, P. A.; Johnson, D. K., Cellulose crystallinity index: measurement techniques and their impact on interpreting cellulase performance. *Biotechnol. Biofuels* **2010**, *3*.
(46) Misiego, C. R.; Pipes, R. B. Dispersion and its relation to carbon nanotube concentration in polyimide nanocomposites. *Compos. Sci. Technol.* **2013**, *85*, 43−49.
(47) Lewin, M. *Handbook of Fiber Chemistry*; CRC/Taylor & Francis: New York; Boca Raton, 2007.
(48) He, X.; Xiao, Q.; Lu, C. H.; Wang, Y. R.; Zhang, X. F.; Zhao, J. Q.; Zhang, W.; Zhang, X. M.; Deng, Y. L. Uniaxially aligned electrospun all-cellulose nanocomposite nanofibers reinforced with cellulose nanocrystals: scaffold for tissue engineering. *Biomacromolecules* **2014**, *15*, 618−627.
(49) Li, Y. J.; Ko, F. K.; Hamad, W. Y. Effects of emulsion droplet size on the structure of electrospun ultrafine biocomposite fibers with cellulose nanocrystals. *Biomacromolecules* **2013**, *14*, 3801−3807.
(50) Liao, H. Q.; Wu, Y. Q.; Wu, M. Y.; Zhan, X. R.; Liu, H. Q. Aligned electrospun cellulose fibers reinforced epoxy resin composite films with high visible light transmittance. *Cellulose* **2012**, *19*, 111−119.
(51) Martinez-Sanz, M.; Olsson, R. T.; Lopez-Rubio, A.; Lagaron, J. M. Development of bacterial cellulose nanowhiskers reinforced EVOH composites by electrospinning. *J. Appl. Polym. Sci.* **2012**, *124*, 1398−1408.
(52) Uddin, A. J.; Araki, J.; Gotoh, Y. Characterization of the poly(vinyl alcohol)/cellulose whisker gel spun fibers. *Composites, Part A* **2011**, *42*, 741−747.
(53) Rusli, R.; Eichhorn, S. J. Determination of the stiffness of cellulose nanowhiskers and the fiber-matrix interface in a nanocomposite using Raman spectroscopy. *Appl. Phys. Lett.* **2008**, *93*, 033111.